Surrogate Modeling Accelerated Shape Optimization of Deployable Composite Tape-Spring Hinges

Hao Jin* and Qilong Jia†
Xi'an Jiaotong University, 710049 Xi'an, People's Republic of China
Ning An‡
Sichuan University, 610065 Chengdu, People's Republic of China
Guiping Zhao§
Xi'an Jiaotong University, 710049 Xi'an, People's Republic of China
Xiaofei Ma¶
Xi'an Institute of Space Radio Technology, 710100 Xi'an, People's Republic of China
and
Jinxiong Zhou**
Xi'an Jiaotong University, 710049 Xi'an, People's Republic of China

https://doi.org/10.2514/1.J061668

Composite tape-spring hinge (CTSH) is a simple yet elegant mechanical component for various deployable space structures. This paper formulates and addresses cut-out shape optimization of a CTSH, which is seldom touched upon in literature. Both the maximum strain energy stored during the folding process as well as the maximum bending moment during deployment were maximized in a concurrent way, and the multi-objective optimization problem was realized by merging data-driven surrogate modeling and shape optimization. Four different surrogate modeling techniques (radial basis function, kriging, Gaussian process regression, and artificial neural network) are evaluated and compared. The maximum stored strain energy at the fully folded state and the maximum bending moment during deployment for the optimal CTSH are increased by 50 and 35%, respectively, compared to the initial design under a previously developed composite failure criterion as constraint. To ensure reproducibility and foster future research, we publicly share our full implementation with the source codes and trained models with the community.

Nomenclature

A, B, C	=	reference points for boundary conditions
ABD	=	constitutive matrix
D	=	diameter of the end circle, mm
E_m	=	elastic modulus of resin, MPa
E_s	=	stored strain energy, mJ
$E_s^{\max}$	=	maximum stored strain energy, mJ
E_1	=	longitudinal stiffness of tow, MPa
E_2, E_3	=	transverse stiffnesses of tow, MPa
F_x, F_y	=	in-plane failure strengths, combination of failure coefficients
F_{1c}, F_{2c}	=	compressive strength parameters
F_{1t}, F_{2t}	=	tensile strength parameters
F_3, F_4, F_6	=	in-plane shear, bending, and twisting strength parameters
FI_c	=	critical value of the failure index
FI_1	=	in-plane failure index
FI_2	=	bending failure index
FI_3	=	coupled in-plane and bending index
f_i, f_{ij}	=	failure coefficients, combination of strength parameters
G_{12}, G_{13}	=	shear stiffnesses of tow, MPa
G_{23}	=	in-plane shear stiffness of tow, MPa
L	=	slot length, mm
M_d	=	bending moment, N · mm
$M_d^{\max}$	=	maximum bending moment, N · mm
P_0, P_1, P_2, P_3	=	control points of the cut-out shape
R^2	=	correlation coefficient
S_f	=	safety factor
W	=	slot width, mm
x_1, x_2, x_3, y_1, y_2	=	coordinates of the control points, mm
θ_i^j	=	rotation freedom degree about the i axis on j point, $i \in \{x, y, z\}$, $j \in \{\mathrm{A}, \mathrm{B}, \mathrm{C}\}$
κ_l	=	longitudinal curvature, 1/mm
κ_t	=	transverse curvature, 1/mm
υ_m	=	Poisson's ratios of resin
υ_{12}, υ_{13}, υ_{23}	=	Poisson's ratios of tow

Received 25 January 2022; revision received 20 May 2022; accepted for publication 12 June 2022; published online 5 July 2022.

*Ph.D. Candidate, State Key Laboratory for Strength and Vibration of Mechanical Structures and School of Aerospace.
†Ph.D., State Key Laboratory for Strength and Vibration of Mechanical Structures and School of Aerospace.
‡Associate Professor, School of Aeronautics and Astronautics; anning@scu.edu.cn (Co-Corresponding Author).
§Professor, State Key Laboratory for Strength and Vibration of Mechanical Structures and School of Aerospace.
¶Research Fellow.
**Professor, State Key Laboratory for Strength and Vibration of Mechanical Structures and School of Aerospace; jxzhouxx@mail.xjtu.edu.cn (Corresponding Author).

I. Introduction

COMPOSITE tape-spring hinge (CTSH), which is also known as composite tube hinge, is a thin-walled cylindrical tube consisting of two opposite and parallel cut-out slots that is commonly made of high-strain composite laminates by laser cutting. The cut-out design of a CTSH allows it to be folded elastically into a small volume before and during launch and then unfolded by releasing the stored strain energy for use once in orbit. The CTSH has been developed and employed as one of the most fundamental mechanical components for constructing large-scale space structures due to its advantages, such as being lightweight and low cost. A CTSH serves as a flexible "joint," e.g., joining two large panels by their edges, and a large-scale space structure usually consists of many such joints, which makes it possible to pack a really large structure into a very small volume. The most well-known application example of CTSHs in a space mission is the antennas on MARSIS, the Mars Express

Spacecraft launched by the European Space Agency (ESA) in June 2003. The MARSIS antennas employed a total of three composite booms, and each of the booms consists of a number of CTSHs to be folded for compact storage before launch [1,2]. Then, after a two-year journey, in the summer of 2005, the booms were ultimately deployed by removing the constraints, thus releasing the strain energy stored in the folded CTSHs and allowing the booms to return to their original deployed state. Additionally, several other design concepts for solar arrays and antennas have also been proposed based on the use of CTSHs, such as the three-parallel-slot CTSH [3], the triangular prism mast [4], the integral folding hinges (IFH) in the support structure concept [5,6], the nonplanar support structure design for deployable reflectors [7], and the self-deployable truss of a novel space telescope [8].

Considering the application scenarios of the CTSH, most previous studies involve analyzing and evaluating its folding and deployment performance. The performance of a CTSH could be characterized by two basic measures, i.e., the strain energy stored during the folding process and the bending moment exported by the CTSH during deployment. Generally, it is expected to obtain a better deployment performance if more elastic energy could be stored in the stowed state since the subsequent deployment is driven by releasing the stored energy. Although an analytical model has already been formulated to determine the quasi-static moment–rotation relationship for the single-layer tape-spring two decades ago [9,10], there are several limitations that prevent its extension into the analysis of more complex laminated structures like CTSHs. As a result, numerical simulation is alternative to the analytical approach to analyze and evaluate the performance of CTSHs and can be substituted for costly physical experiments. Over the past decades, a substantial number of computational models have been developed for simulating the folding and unfolding process of CTSHs, and commercially available finite element packages such as Nastran, Ansys, LS-Dyna, and Abaqus [1,2,11–13] have been widely used to facilitate the interaction between industry and academia. Among them, Abaqus takes on a powerful feature for analyzing the highly nonlinear behavior (i.e., large geometric changes accompanied by buckling and dynamic snapping, etc.) of the CTSHs. Abaqus/Explicit solver has proven valuable in solving both the quasi-static folding/unfolding and dynamic deployment problems, as well as the built-in Python scripting interface eases the automatic generation and calculation of finite element models [14]. Mallikarachchi and Pellegrino [13,15] provided the first comparison between Abaqus/Explicit quasi-static folding and deployment simulation results and the experimentally measured behavior of a tape-spring hinge made from carbon-fiber-reinforced plastic (CFRP) composite. It is shown that not only the numerical model has successfully and quantitatively captured the highly nonlinear behavior such as buckling and snapping of CTSHs observed in experiments, but also the numerical model provides more details about the stress redistribution and strain energy variations during the process, which are not easy to be measured through experiments. Moreover, several experimentally based failure criteria have been developed to predict the failure behavior of thin-ply CFRP laminates [16–19], and implementing these models into finite element models allows for the prediction of failure strength of CTSHs.

Structural optimization design is also an important work in CTSH research. In 2016, ESA started a project to develop novel elastic hinge concepts for composite arms of deployable antennas. One of the main challenges in designing the elastic hinges is that there are two opposing requirements that need to be balanced here, i.e., flexibility to sustain high-strain deformations and rigidity to support external loads and/or reach certain natural frequencies [20,21]. Therefore, rigorous optimization research is required to find the optimal cut-out design for CTSHs. It is quite straightforward to implement an optimization procedure by combining numerical simulations with optimization algorithms; in fact, many efforts have been devoted to this area. Mallikarachchi and Pellegrino [22] carried out a sensitivity analysis in order to analyze the effect of some geometric parameters such as the slot length, width, and end circle diameter on the quasi-static folding and deployment performance of composite tube hinges. Ye et al. [23] proposed an optimal design approach combining a response surface methodology (RSM)-based model with a large-scale generalized reduced gradient (LSGRG) optimization algorithm for a self-locking tape-spring under pure bending, and reported a 19.5% increase in the steady-state moment while satisfying the maximum stress constraint. Yang et al. [24] performed a multi-objective optimization design study of the double-layer metallic tape-spring hinge using the modified nondominated sorting genetic algorithm (NSGA-II) algorithm, where the steady-state moment and peak moment of the hinge quasi-static deployment are selected as two optimization objectives. Liu et al. [25] established an optimization problem for CTSHs to obtain three conflicting objectives: minimizing the peak folding moment, maximizing the peak torsional moment, and minimizing the mass. However, most of the previous studies have focused on the size optimization of cut-out slots, and the research on the shape and topology optimization of CTSHs remains largely unexplored. The only closely related study focuses on deployable thin shells forming a 90° joint, in which two methods (a level-set function approach for topology optimization and a spline representation for shape optimization) were developed to design cutouts that allow damage-free folding of the stiffest possible design with complex shapes [8].

High-fidelity finite element (FE) analysis of complicated composite structures can be computationally expensive, particularly in the process of optimization design where a large number of objective function evaluations and design sensitivity analyses are involved. Consequently, approximate metamodels or surrogate models are becoming widely used in structural design [26–30]. These approximate models express the relationship between the objective functions (outputs) and the design variables (inputs) with a simple explicit function or a black-box function, enabling dramatic saving of computational cost and exploration of a wider design space. Popular surrogate models include response surface, kriging, neural networks, radial basis functions (RBFs), support vector or Gaussian process regression (GPR), and moving least squares, among others [26–30]. Modeling quasi-static folding and deployment process of CTSH is a highly nonlinear process and is hard to converge. It is alternatively solved by using a dynamic/explicit solver, but a high computational cost, e.g., hours of computation for each case, has to be borne for convergence. This becomes the biggest concern for structural optimization problems where hundred or thousand times of structural response calculations are involved. Developing much cheaper surrogate models to replace high-fidelity simulations is desperately needed. For such a complicated problem of practical importance, it is intriguing to use and compare various surrogate models for the problem.

The main novelty of this work is that it tries to establish a surrogate modeling-accelerated optimization procedure for finding the optimal cut-out shape and maximizing the folding and deployment performance of CTSH without causing any material failure. We firstly develop a dynamic FE modeling scheme to simulate the quasi-static folding and deployment behavior of CTSH subjected to rotation about a transverse axis. A parametric study was conducted by analyzing the effect of the cut-out size on the performance of the CTSH, and a well-established failure criterion was introduced to estimate the failure of the CTSH. We then formulate a multi-objective shape optimization problem of the CTSH to concurrently maximize the stored strain energy during folding and the maximum deployment moment during deploying without causing failure of materials. The cut-out shape was represented by a cubic spline and the coordinates of control points of the spline were taken as design variables. Four different data-driven surrogate modeling techniques were used to correlate the relation between the design variables and objectives, and a comparison was made among them. Finally, the surrogate model was substituted into a genetic algorithm (GA)-based optimizer, and the optimized shape obtained by this procedure demonstrates 50 and 35% increase in the maximum stored energy and peak bending moment, respectively.

This paper is organized as follows. The FE model of the CTSH as well as its folding and deployment behavior are described in Sec. II. Emphasis is paid to the effect of simple shape variation by changing one geometric size of the cut on the behavior of CTSH, implying the importance of shape optimization. Section III gives a rigorous mathematical formulation of a multi-objective optimization problem. The surrogate modeling technology used in this study and a detailed

implementation of the optimization problem are given in Sec. IV. The optimization results are discussed in Sec. V. Finally, some concluding remarks are given in Sec. VI.

II. Mechanical Behavior and Failure Mechanism of CTSH

Figure 1 presents the fully deployed stress-free state (a) and the stowed state (b) of the CTSH. The CTSH was manufactured by cutting two opposite and parallel slots into a thin-walled composite tube with a diameter of 38 mm. The slot shape of the initial design is characterized by the diameter of the end circle, D; the slot length L; and the slot width W. The geometry of the slot is symmetric with respect to the longitudinal and circumferential axes passing through the center of the slot. In the following simulation, the geometry of the initial design is fixed to be $D = 28$ mm, $L = 66$ mm, and $W = 10$ mm.

We are concerned with the folding and deployment process of the CTSH. To model the whole process, appropriate boundary conditions need to be specified. Figure 2 shows the boundary conditions adopted herein. Two end cross sections are assumed to be kinematically rigid, which is realized by coupling the nodes on the two sections to reference points A and B, respectively. For the section referenced with point A, only rotation about the x axis, θ_X, is allowed; for the section referenced with point B, θ_X and U_X^C are permitted. The rotational degrees of freedom about the x axis of point A and point B are correlated to a dummy point C, and a rotation θ_X^C is prescribed to induce the folding of the hinge. The hinge was discretized by four-node reduced integration shell element (S4R) with a global element size of 3.0 mm. The simulation was carried out by using the Dynamic/Explicit solver in the nonlinear commercial FE code Abaqus 2020. Quasi-static conditions were ensured by monitoring the model energy variations throughout the whole simulation. A detailed dynamic finite element procedure for calculating the quasi-static buckling and collapsing of thin-walled tubular composite structures can be found in our recent paper [31]. Modeling the whole folding-unfolding process is time-consuming, and the running typically takes about 3 h to complete in a PC with AMD Ryzen 7 3700X 8-Core CPU at 3.59 Hz. Optimization of this hinge is thus prohibitively computer-intensive, and surrogate modeling is desperately needed.

The CTSH is made from a two-ply ±45 plain-weave laminate (T300-1k/913 tow and HexPly 913 resin), with an areal density of 260 g/m^2 and the 0° direction corresponding to the cylinder's axis. The material parameters used in the simulation are taken from [13] and summarized as follows: $E_1 = 159{,}520$ MPa, $E_2 = E_3 = 11{,}660$ MPa, $G_{12} = G_{13} = 3813$ MPa, $G_{23} = 3961$ MPa, $v_{12} = v_{13} = 0.27$, $v_{23} = 0.47$, and $\rho = 1.6 \times 10^{-6}$ kg/mm^3 for tow; and $E_m = 3390$ MPa and $v_m = 0.41$ for resin. The elastic stiffness of this specific laminate could be modeled with a constitutive matrix ABD, shown in Eq. (1), according to a modified classical lamination theory proposed by Mallikarachchi and Pellegrino [13]. The total length of the hinge was set to be 220 mm, and 3300 elements were used to discretize the hinge. A mesh independence was checked before detailed simulation and optimization.

$$ABD = \left(\begin{array}{ccc|ccc} 7714 & 6380 & 0 & 0 & 0 & 0 \\ 6380 & 7714 & 0 & 0 & 0 & 0 \\ 0 & 0 & 5962 & 0 & 0 & 0 \\ \hline 0 & 0 & 0 & 23.6 & 19.1 & 0 \\ 0 & 0 & 0 & 19.1 & 23.6 & 0 \\ 0 & 0 & 0 & 0 & 0 & 19.9 \end{array}\right) \quad (1)$$

where the units are newtons and millimeters.

The failure mechanism of composite materials is a long-standing topic that is far from mature, and a considerable amount of research,

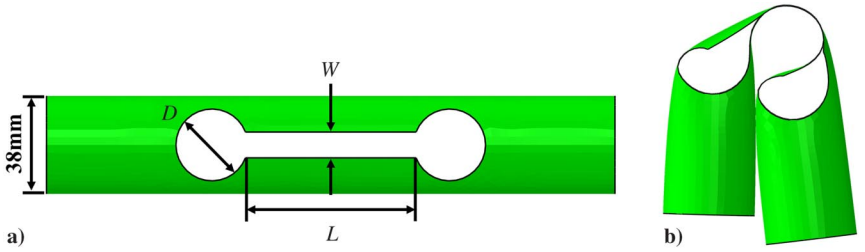

Fig. 1 Schematics of the CTSH: a) fully deployed, i.e., unstressed configuration, and b) folded, i.e., stressed configuration.

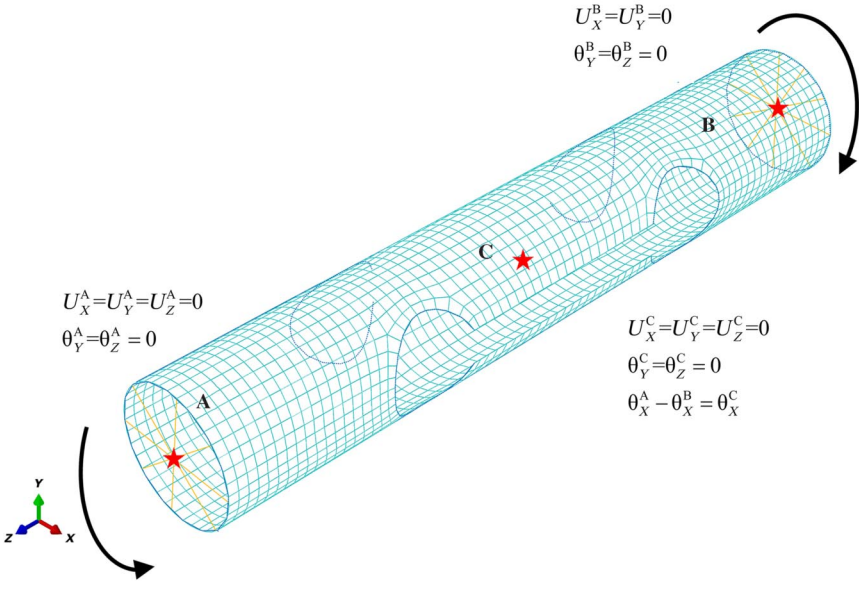

Fig. 2 Finite element model of CTSH with mesh representation and boundary conditions.

either experimental or theoretical, has already taken place. In this study, the failure criterion proposed by Mallikarachchi and Pellegrino [17] was adopted because it has proven useful for predicting the material failure of two-ply plain-weave carbon fiber laminates and has been successfully applied to solve the topology and shape optimization problem for a thin-walled composite deployable joint structure in a recent work [8]. This criterion can be expressed in terms of six forces and moment stress resultants $N_x, N_y, N_{xy}, M_x, M_y$, and M_{xy} with a set of three inequalities related to in-plane, bending, and coupled in-plane and bending failure types, described as follows:

$$\begin{cases} FI_1 = f_1(N_x + N_y) + f_{11}\left(N_x^2 + N_y^2\right) + f_{12}N_xN_y + f_{33}N_{xy}^2 < 1 \\ FI_2 = f_{44} \times \max\left(M_x^2, M_y^2\right) + f_{66}M_{xy}^2 < 1 \\ FI_3 = \max\left(\dfrac{N_x}{F_x}, \dfrac{N_y}{F_y}\right) + \dfrac{\max(|M_x|, |M_y|)}{F_4} < 1 \end{cases} \tag{2}$$

where the failure coefficients f_i and f_{ij} are given by

$$\begin{cases} f_1 = f_2 = \dfrac{1}{F_{1t}} - \dfrac{1}{F_{1c}}, f_{11} = f_{22} = \dfrac{1}{F_{1t}F_{1c}}, f_{12} = -\dfrac{f_{11}}{2} \\ f_{33} = \dfrac{1}{F_3^2}, f_{44} = f_{55} = \dfrac{1}{F_4^2}, f_{66} = \dfrac{1}{F_6^2} \end{cases} \tag{3}$$

and

$$\begin{cases} F_x = \dfrac{-(f_1+f_{12}N_y) \pm \sqrt{(f_1+f_{12}N_y)^2 - 4f_{11}(f_1N_y + f_{11}N_y^2 + f_{33}N_{xy}^2 - 1)}}{2f_{11}} \\ F_y = \dfrac{-(f_1+f_{12}N_x) \pm \sqrt{(f_1+f_{12}N_x)^2 - 4f_{11}(f_1N_x + f_{11}N_x^2 + f_{33}N_{xy}^2 - 1)}}{2f_{11}} \end{cases} \tag{4}$$

where F_i represent directly measured strengths in the tow directions of the laminate, and the subscripts t and c denote tension and compression, respectively. In light of the fact that the same woven composite was used, we will take the strength parameters reported in [32] as shown in Table 1.

To begin with, we focus on analyzing the failure mechanism of the initial design of CTSH characterized by $L = 66$ mm, $W = 10$ mm, and $D = 28$ mm. In Fig. 3a we report the evolution of the three failure indices FI_1, FI_2, and FI_3 of all CTSH elements as a function of folding angle during the quasi-static folding process. It is shown that all the three indices show a rising trend as the hinge is being folded from 0 toward 180 deg. Specifically, the values of FI_2 and FI_3 approach and even exceed the failure critical value of 1.0 at the fully folded state; in sharp contrast, the value of FI_1 is far below the threshold during the whole process. Given also that both FI_2 and FI_3 reach their maxima at the fully folded state, we will focus on the failure indices values of FI_2 and FI_3 at the fully folded state in the reminder of this paper. Figure 3b gives the distribution of the three failure indices at several typical folded angles in the process, i.e., 45, 90, and 172 deg. It is clearly that the maxima of all three indices occur in the cut-out edge regions, therefore emphasizing the importance of cut-out shape optimization.

Table 1 Material strength parameters for two-ply laminates of T300-1k/913 tow and HexPly 913 resin [32]

Strength parameter	Value
$F_{1t} = F_{2t}$, N/mm	139.47
$F_{1c} = F_{2c}$, N/mm	63.42
F_3, N/mm	17.73
$F_4 = F_5$, N/mm	5.07
F_6, N/mm	1.53

We then perform a parametric study to quantify the effect of cut-out geometry design on the folding and unfolding performance, as well as the failure mechanisms of CTSH. The results are given in Fig. 4. A variety of geometry designs were generated by varying the diameter of cut-out end circles, D, ranging from 10 to 28 mm, while the slot length L and width W remained unchanged. Figure 4a plots the strain energy stored in the folding process, E_s, versus folding angle from 0 to 172 deg. When the folding process completes, the deployment process follows. Figure 4b plots the bending moment M_d versus the deployment angle curve, where M_d is extracted as reaction moment when the folding angle is prescribed and varied from 172 to 0 deg. It is shown from Figs. 4a and 4b that, smaller end circles are preferred in order to improve the deployment performance, namely, to obtain a higher strain-energy stored in the folded state and a larger peak moment during the deployment process. However, the reduction in the cut-out size would on the other hand increase the risk of failure. Figure 4c plots the maximum values of the three failure indices FI_1, FI_2, and FI_3. As can be seen, all the three failure indices increase as the end circle diameter D decreases, and all of the designs presented here are not safe because the values of FI_2 and FI_3 are both greater than 1.0. These issues, therefore, necessitate careful optimization of CTSH for finding an optimized cut-out shape that maximizes the deployment performance without causing failure of materials. Finally, we would like to note that varying the size of D in Fig. 4 is somehow similar to the cut-out size optimization study in a previous work [22], but it is not the shape optimization discussed below, though.

III. Formulation of Multi-Objective Shape Optimization Problem

We now describe the multi-objective shape optimization problem of the CTSH, which is illustrated in Fig. 5. Figure 5a shows a zoom-in picture of the local boundary shape to be optimized. A number of controlling points, e.g., P_0, P_1, P_2, and P_3, are selected along the boundary of interest, and the boundary shape is approximated via interpolation through these controlling points. Specifically, a cubic spline interpolation through the four controlling points is used to describe the local shape of the half end circle as shown in Fig. 5a, and symmetry is preserved for the remaining half circle. Thus the shape optimization problem can be formulated by using the coordinates of controlling points as design variables, which is a common practice in many shape optimization problems [8,33,34]. During optimization, P_0 is fixed and P_3 is only allowed to move along the x axis; P_1 and P_2 are allowed to move, respectively, within two areas enclosed by the dotted line box. Therefore, the number of design variables is five, i.e., x_1, y_1, x_2, y_2, and x_3.

For practical design of the folding and deployment of CTSH, several concerns should be incorporated into one successful design, resulting in a multi-objective optimization problem with constraints. The stored strain energy, denoted by E_s, is one physical parameter closely related to the performance of CTSH: the strain energy represents the capability of the CTSH for following deployment, and the larger the E_s, the greater the capability to deploy. Figure 5b plots the E_s versus folding angle curve during the whole folding process when folding angle was varied from 0 to 172 deg. The stored strain energy E_s shows an overall increase trend as a function of the folding angle, and the maximum $E_s^{\max}$ is recorded. During the deployment process, the bending moment M_d versus deployment angle curve is shown in Fig. 5c and the maximum bending moment $M_d^{\max}$ is highly desirable. Thus, two objective functions $E_s^{\max}$ and $M_d^{\max}$ should be concurrently maximized. Note that an admissible safe design is guaranteed only if the design of CTSH satisfies the failure criterion given beforehand. To summarize, a rigorous mathematical formulation of the multi-objective shape optimization for CTSH can be given as

$$\begin{cases} \text{Find}: x_1, x_2, x_3, y_1, y_2 \\ \text{Maximize}: M_d^{\max} \text{ and } E_s^{\max} \\ \text{Subject to}: FI_i < FI_c * S_f, i = 1, 2, 3 \end{cases} \tag{5}$$

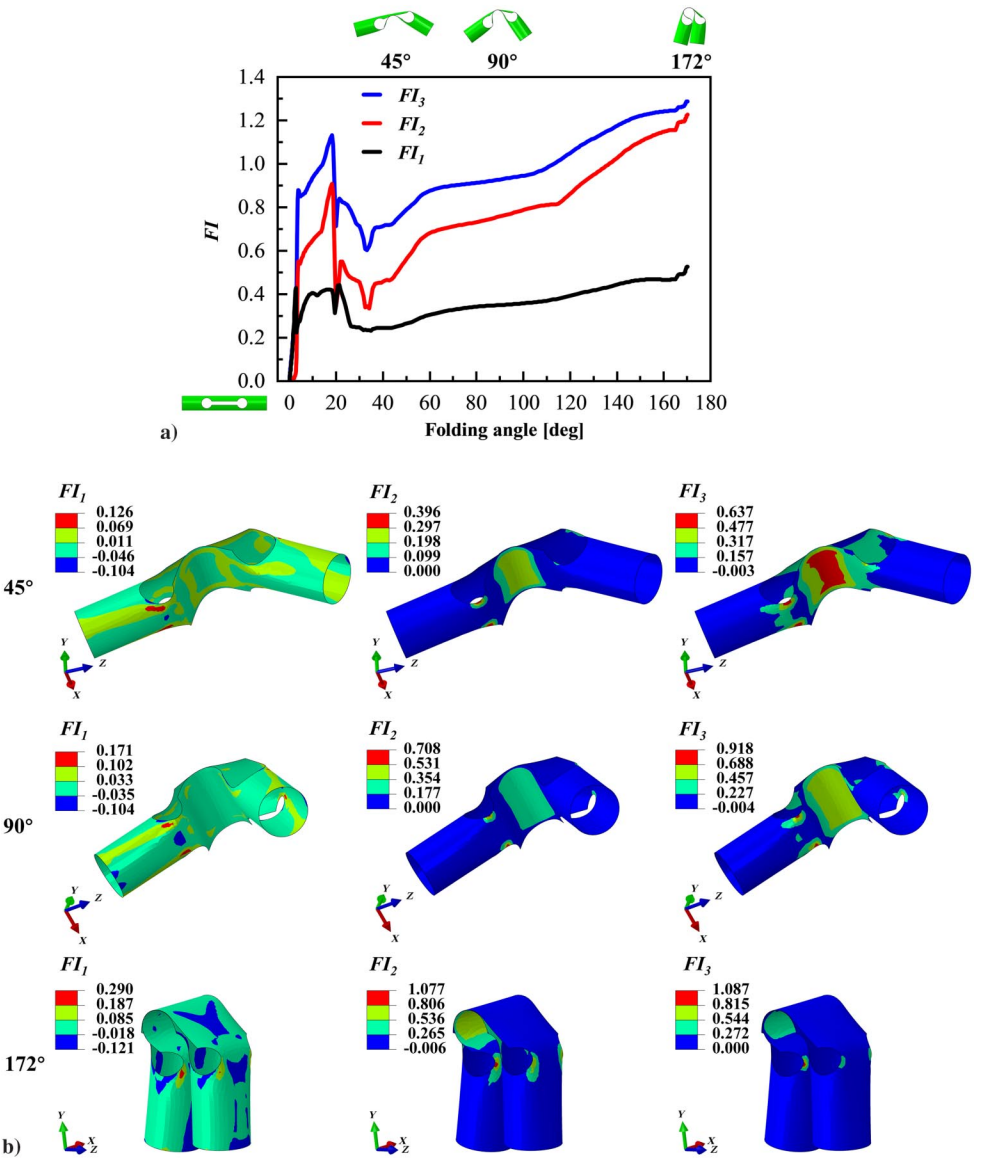

Fig. 3 Failure mechanism of CTSH: a) the maximum failure indices FI_i versus the folding angle, and b) deformation snapshots showing FI_i distribution.

where the x_1, x_2, x_3, y_1, and y_2 are the five design variables, which are, respectively, allowed to vary in the following ranges: $x_1 \in [45, 60]$, $x_2 \in [60, 75]$, $x_3 \in [60, 75]$, $y_1 \in [5, 15]$, and $y_2 \in [5, 15]$, as shown in Fig. 5a. $M_d^{\max}$ is the peak moment during deployment, and the $E_s^{\max}$ is the maximum stored strain energy during folding. These two objective functions are set as the multi-objectives that should be maximized. The failure criterion with three inequalities was used as constraint. Note that $FI_c = 1.0$ is the critical failure value as given in Eq. (2), and a safety factor $S_f = 0.93$ is introduced in our practice to overcome possible prediction errors of surrogate models. The safety factor value is determined through trial and error, which will be discussed later.

IV. Data-Driven Surrogate Modeling and Shape Optimization of CTSH

A. Surrogate-Model-Based Shape Optimization Framework

The surrogate-model-based shape optimization framework consists of four steps, as depicted in Fig. 6. The first step is the design of experiments (DOE), in which the optimal Latin hypercube technique was adopted to create a data set that samples the design space. The sample size is set to 300 according to the trial-and-error method. The DOE study was conducted twice independently: once for the training data and again for the testing data. Second, FE calculations were performed to generate the needed data used for the surrogate model training and testing. Abaqus/Python scripts were developed to automate the simulation run for each sampling point, which take the five design variables as input, run a high-fidelity simulation, and post-process some outputs such as the mass of the hinge, the stored strain energy at fully folded state, the peak moment during deployment, and the failure indices. The third step employs the FE database to develop the surrogate model for quickly predicting the performance of CTSH. Herein, a total of four approaches (RBFs, kriging, GPR, and artificial neural networks [ANNs]) were used to construct the surrogate models. The above-mentioned surrogate models were all implemented in an offline way. Finally, the surrogate model was imported into the optimization software Isight 2020, and the optimization problem was solved by a multi-objective genetic algorithm NSGA-II provided in Isight. We note that the established optimization environment has been demonstrated to be efficient and robust for a wide range of optimization problems, either linear or nonlinear problems. One recent example is the large deformation analysis and shape optimization of soft mechanical metamaterials [33]. To ensure reproducibility and foster future research, we publicize the data and codes for

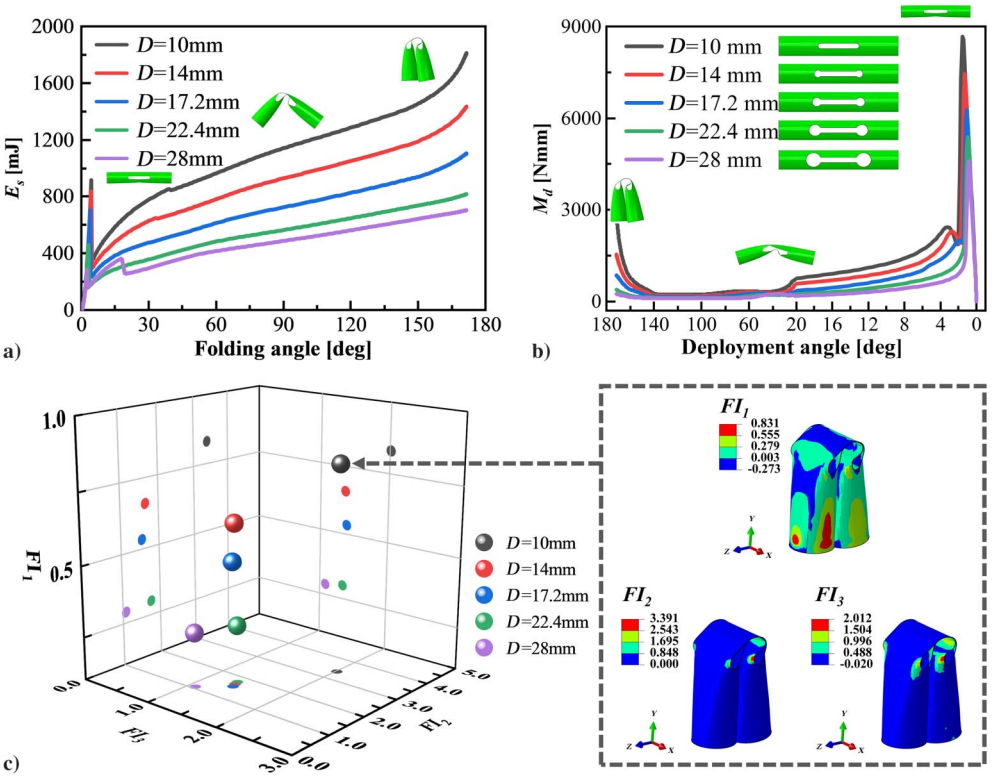

Fig. 4 Mechanical response of CTSH in a quasi-static folding-and-deploying cycle: a) E_s versus folding angle, b) M_d versus deployment angle, and c) distribution of FI_i.

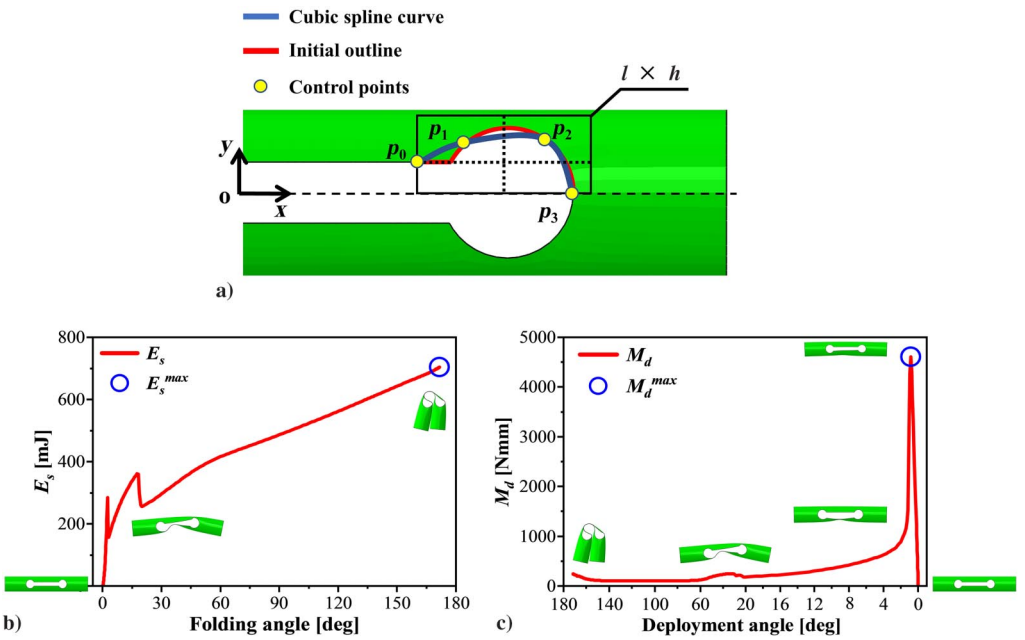

Fig. 5 Shape optimization of CTSH: a) schematic of the controlling points and spline, b) E_s versus folding angle, and c) M_d versus deployment angle.

surrogate modeling and shape optimization of CTSHs via https://github.com/XJTU-Zhou-group/Shape-optimization-CTSH.

B. Construction of Surrogate Models of CTSH

To apply the most accurate surrogate model for optimization tasks, this section compares four surrogate model strategies. Actually, the four surrogate models were constructed in different software environments, which are, respectively, i) Isight for RBF; ii) in-house MATLAB codes for kriging; iii) MATLAB Regression Toolbox for GPR; and iv) Python and TensorFlow library for ANN.

The first surrogate model considered is the RBF model. Given a set of sampling data, $\boldsymbol{x}^{(i)} = \{x^{(1)}, x^{(2)}, \cdots, x^{(n)}\}^T$, and the corresponding observations $\boldsymbol{y}^{(i)} = \{y^{(1)}, y^{(2)}, \cdots, y^{(n)}\}^T$, an RBF approximation $\hat{f}$ is given as

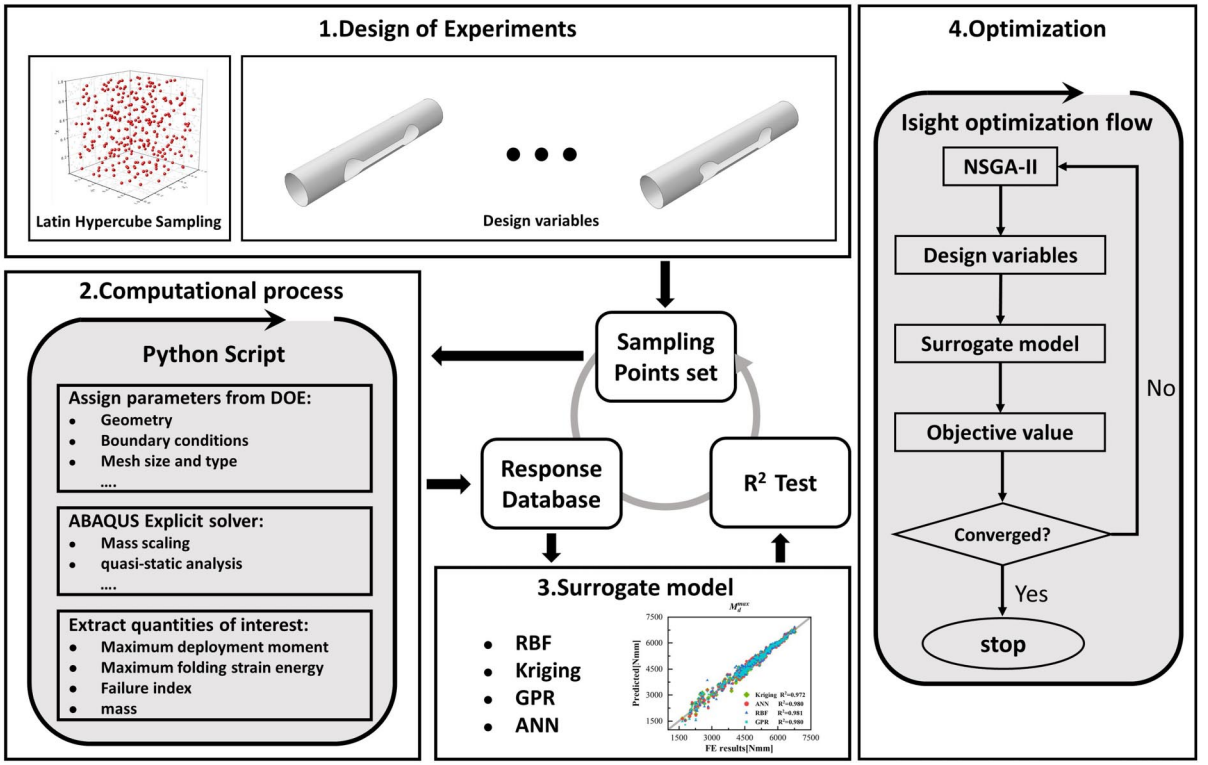

Fig. 6 Flowchart of the surrogate modeling and optimization process.

$$\hat{f}(\boldsymbol{x}) = \boldsymbol{w}^T\Psi = \sum_{i=1}^{n_c} w_i \Psi\Big(\|\boldsymbol{x} - \boldsymbol{x}^{(i)}\|\Big) \tag{6}$$

where $\boldsymbol{x}$ is the prediction site, $\boldsymbol{w}$ are weights, and Ψ is the basis function. The computation of $\boldsymbol{w}$ is simply given as

$$\boldsymbol{w} = \boldsymbol{\Phi}^{-1}\boldsymbol{y} \tag{7}$$

where the so-called Gram matrix is $\Phi_{i,j} = \Psi(\|\boldsymbol{x}^{(i)} - \boldsymbol{x}^{(j)}\|), i, j = 1, 2, \cdots, n$. Various forms of basis functions are available, such as linear, cubic, spline, Gaussian, multiquadric, and inverse multiquadric.

If the basic function in Eq. (6) is given as

$$\Phi^{(i)} = \exp\left(-\sum_{j=1}^{k} \theta_j |x_j - x_j^{(i)}|^{p_j}\right) \tag{8}$$

this gives rise to the kriging model. Kriging allows the exponent ($p_j = \{p_1, p_2, \cdots, p_k\}^T$) to vary for each dimension in $\boldsymbol{x}$, and the appearance of θ_j allows the width of the basis function to vary from variable to variable [26].

In the Gaussian process considered, an approximation $\hat{f}$ can be written as

$$\boldsymbol{y}^{(i)} = f[\boldsymbol{x}^{(i)}] + \varepsilon^{(i)} \tag{9}$$

where $f[\boldsymbol{x}^{(i)}]$ is the unknown function value at $\boldsymbol{x}^{(i)}$ to be approximated by GPR, and $\varepsilon^{(i)}$ is the GPR noise with standard deviation $\sigma_\varepsilon^{(i)}$ that also depends on the input point $\boldsymbol{x}^{(i)}$. If one desires to predict the quantity of interest $\boldsymbol{y}^{(*)}$ at an new input point $\boldsymbol{x}^{(*)}$, then the GPR is written as a multivariate Gaussian distribution:

$$\begin{bmatrix} \boldsymbol{y} \\ \boldsymbol{y}^{(*)} \end{bmatrix} \sim \mathcal{N}\left(\boldsymbol{0}, \begin{bmatrix} \boldsymbol{K} + \boldsymbol{R} & \boldsymbol{k}_* \\ \boldsymbol{k}_*^T & k[\boldsymbol{x}^{(*)}, \boldsymbol{x}^{(*)}] \end{bmatrix}\right) \tag{10}$$

where, $\boldsymbol{y} = [\boldsymbol{y}^{(i)}, \boldsymbol{y}^{(j)}], i \in [1, n], j \in [1, n]$. $\boldsymbol{K}^{i\times j}$ is a matrix constructed by $k[\boldsymbol{x}^{(i)}, \boldsymbol{x}^{(j)}]$. $\boldsymbol{k}_*^T = \{k(\boldsymbol{x}^{(i)}, \boldsymbol{x}^{(*)}) \cdots, k(\boldsymbol{x}^{(n)}, \boldsymbol{x}^{(*)})\}$ is the vector of kernel functions evaluated at all the pairs composed by the n training points and the new point $x^{(*)}$. The predicted mean and variance of the quantity of interest $\boldsymbol{y}^{(*)}$ at the new point are then written as

$$\begin{cases} \text{mean}[\boldsymbol{y}^{(*)}] = \boldsymbol{k}_*^{\mathrm{T}}(\boldsymbol{K} + \boldsymbol{R})^{-1}\boldsymbol{y} \\ \text{cov}[\boldsymbol{y}^{(*)}] = k[\boldsymbol{x}^{(*)}, \boldsymbol{x}^{(*)}] - \boldsymbol{k}_*^{\mathrm{T}}(\boldsymbol{K} + \boldsymbol{R})^{-1}\boldsymbol{k}_* \end{cases} \tag{11}$$

The MATLAB Regression Toolbox provides multiple kernel functions, such as Squared Exponential Kernel, Exponential Kernel, Matern 3/2, Matern 5/2, and Rational Quadratic Kernel [35,36]. In this paper, we use the "Optimizable GRP" technique, which automatically selects the optimal type of kernel function as well as the corresponding optimal hyperparameters to make the fitting accuracy of the agent model as optimal as possible.

ANN is a powerful class of data-driven function approximation algorithm. The ANN for regression is composed of the first and the last layers, with the sum of neurons equal to the number of input and output dimensions, respectively, and a selected number of intermediate hidden layers that can each contain an arbitrary amount of neurons. The output of a layer is known as the activation. The activation from one layer of an ANN is used as the input to the next layer. The activation produced by the jth hidden layer of the ANN is given by

$$z^{(j)} = \sigma(\boldsymbol{W}^{(j)}\boldsymbol{z}^{(j-1)} + \boldsymbol{b}^{(j)}), \quad \forall\ j \in \{1, 2, \cdots, L\} \tag{12}$$

where $\boldsymbol{W}^{(j)} \in \mathbb{R}^{d_j \times d_{j-1}}$ is weight coefficient matrix, $\boldsymbol{b}^{(j)} \in \mathbb{R}^{d_j}$ is bias vector, and d_j is the number of neurons in the jth hidden layer. Note that $\boldsymbol{z}^{(0)}$ is the input $\boldsymbol{x}^{(i)} = \{x^{(1)}, x^{(2)}, \cdots, x^{(n)}\}^T$, $\boldsymbol{z}^{(L)}$ is the output $\boldsymbol{y}^{(i)} = \{y^{(1)}, y^{(2)}, \cdots, y^{(n)}\}^T$, $d_0 = n$, σ is a nonlinear function applied elementwise on its arguments. Popular choices for σ include the logistic function, the hyperbolic tangent function, or the rectified linear unit (or ReLU) function [37,38]. In this paper, the ANN model

consists of four fully connected (FC) layers (an input layer, an output layer, and two hidden layers). The hidden layers have 64 neurons. The input and output layers include five and four neurons, respectively, equal to the size of input and output data. Rectified linear unit (ReLU) was adopted as the activation function in all hidden layers and input layer. We trained the network using the Adam optimizer. Once the construction of a surrogate model is completed, it is crucial to evaluate the accuracy of the approximation. The so-called R^2 correlation coefficient is evaluated at m test points as

$$R^2 = 1 - \frac{\sum_{i=1}^{m} (y_i - \tilde{y}_i)^2}{\sum_{i=1}^{m} (y_i - \bar{y})^2} \tag{13}$$

where y_i is the test data of the ith sample point, $\tilde{y}_i$ is the surrogate model prediction at the locations of the test data, and $\bar{y}$ is the mean value of y_i, $i = 1, 2, \cdots, m$.

V. Results

As discussed above, four surrogate modeling techniques are adopted for quick prediction of the performance of CTSH. Figure 7 plots the predictions given by the four surrogate models as well as the true FE results. The straight line corresponds to perfect prediction with zero errors. The degree of data scattering and deviation from the straight line is quantitatively characterized by the R^2 measures inserted in each figure. In general, the closer the R^2 to 1, the more accurate the surrogate. The performance of surrogate models is excellent in terms of $M_d^{\max}$, $E_s^{\max}$, and mass, all yielding R^2 measures greater than 97%; while the discrepancy between prediction and test data for failure indices is little bit bigger, but at least 70% R^2 measure is obtained except the worst kriging approximation. It should be pointed out that an as high as possible fitting accuracy is always pursued for the surrogate-model-aided optimization work; however, even a tiny improvement in the fitting accuracy can require a large increase in the data size used for training the model [39], which will lead to an excessive computational cost. The use of an insufficiently accurate surrogate model may result in an inappropriate estimation of CTSH performance. Our approach to overcome this issue is to introduce a safety factor for the failure critical value as has been described in Sec. III.

Figure 8 presents the optimization results obtained by the developed surrogate-model-based framework. Since the four surrogate models give similar approximations as described above, only the ANN-predicted optimal solution was shown here for concise display. The optimal cut-out shape design along with the initial shape of CTSH is given in Fig. 8a. Most recently, when this work was under review, we found that a concurrent work [21] had reported a similar optimization-resulted shape design of CTSH, where the objective of their optimization was to maximize its natural frequency and no surrogate model was used. We should admit that the composite designs with sharp corners given by the present optimization, in particular the spline boundary shape approximation, are only doable for laboratory demonstration. This artifact of optimal boundary shape can be remedied by increasing more boundary nodes for spline approximation or by using higher-order boundary interpolation schemes. Figures 8b–8d plot the convergence curves of NSGA-II for finding the optimal solution, indicating that the two objectives (i.e., $M_d^{\max}$ and $E_s^{\max}$) as well as the constraints (i.e., FI_1, FI_2, and FI_3) gradually converge after 20,000 iterations. We remind that, in order to complete these iteration runs, only 600 FE simulation runs are needed to generate the data used for the training and testing of the surrogate models. And given the fact that the time spent in training and calling surrogate models is negligible compared with the high-fidelity FE calculations, therefore, we highlight that a substantial computation time saving, (20,000-600)/20,000 = 97%, is achieved for this particular problem. Furthermore, it is worth noting that FI_3 was the largest of the three failure indices and also the only one approaching the threshold value. In Table 2 we present comparison among the cut-out shape optimization results obtained by using different surrogate models. Each of the surrogate-model-predicted optimal solution was validated by performing a high-fidelity FE simulation. It can be seen that by taking a safety factor of 0.93 for the failure indices, apart from kriging, the optimal designs obtained by other surrogate models are all proven to be safe and effective. This is consistent with the findings from Fig. 7 that kriging has the worst prediction accuracy among others for this particular problem considered herein.

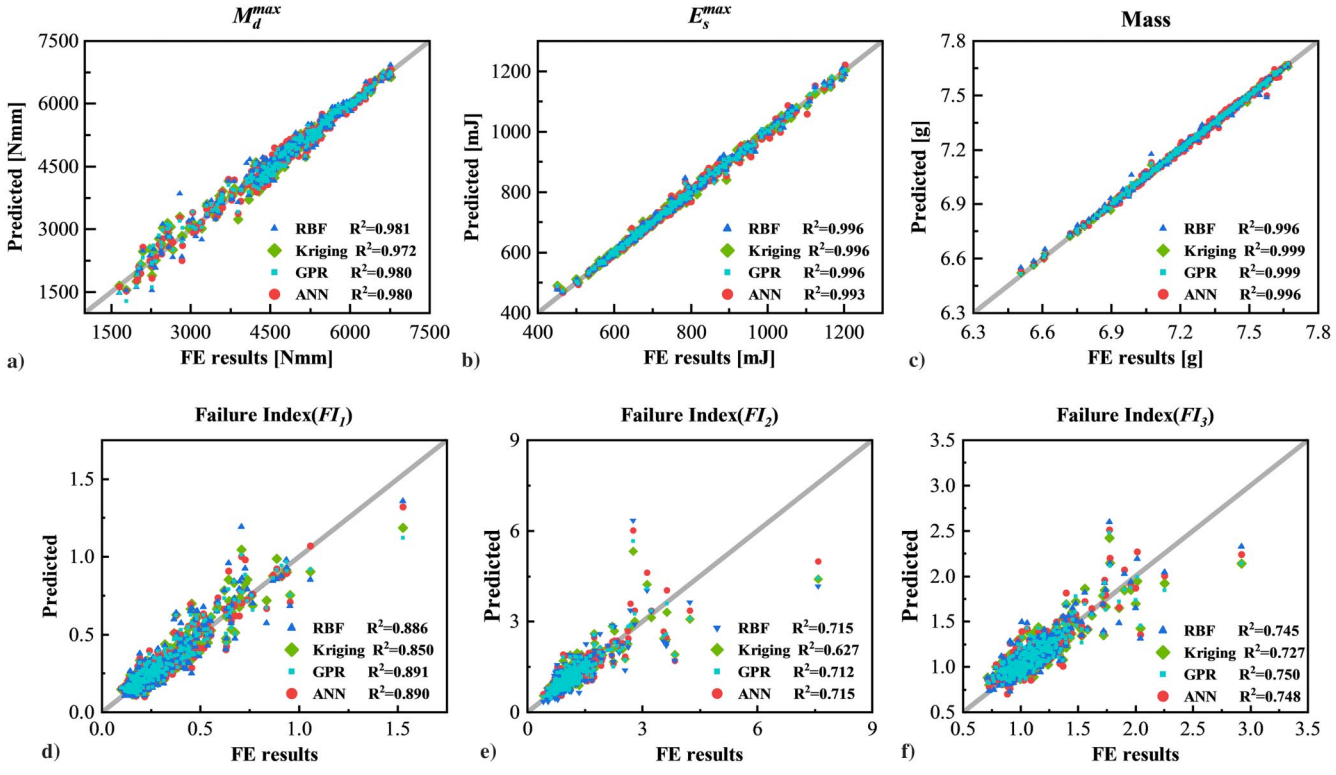

Fig. 7 Evaluation of the performance and accuracy of four used surrogate modeling techniques (RBF, kriging, GPR, and ANN).

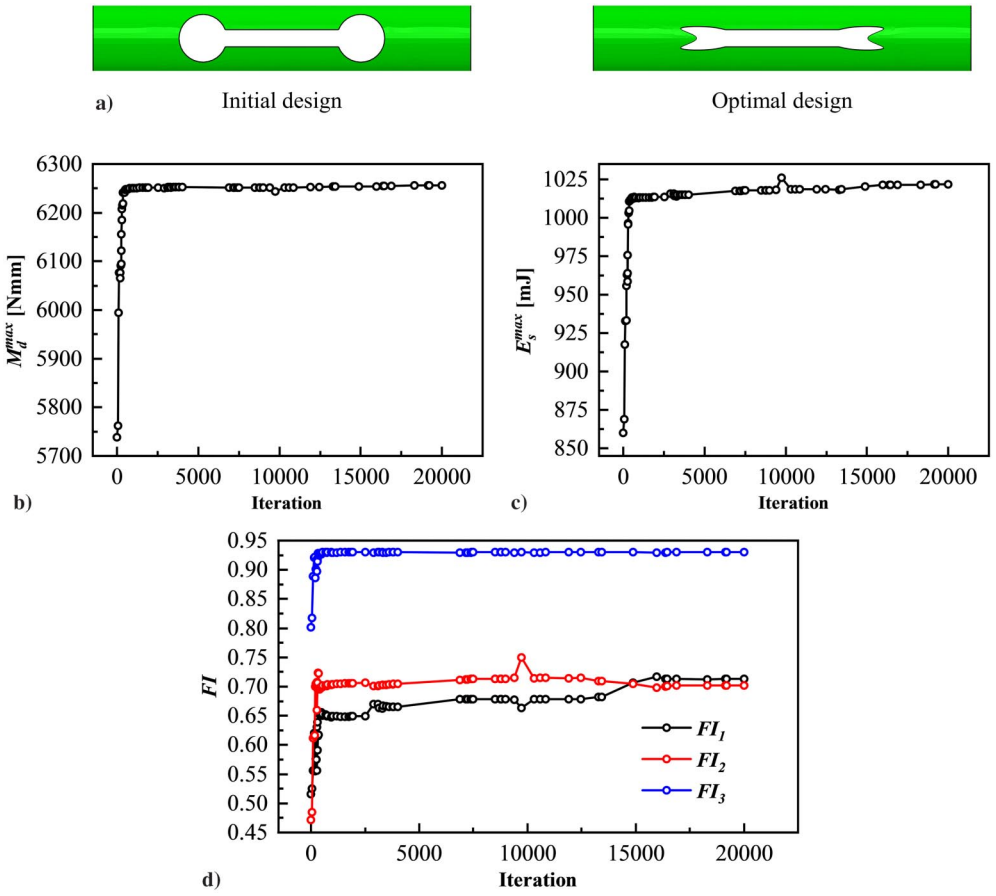

Fig. 8 Optimal cut-out shape design obtained through shape optimization: a) initial and optimized designs, and iteration of b) $E_s^{\max}$, c) $M_d^{\max}$, and d) FI_i.

Next, Fig. 9 presents the comparison between the folding and deployment performance of the initial and optimal design. It can be seen from Figs. 9a and 9b that both the stored strain energy during the folding process and the peak moment during deployment show a significant increase for the optimal design compared to the initial. Specifically, Table 3 summarizes and compares the initial and the optimal designs: $E_s^{\max}$ increases from 699.98 to 1051.20 mJ, $M_d^{\max}$ increases from 4638.89 to 6328.60 N · mm, and the mass of the structure also increases slightly from 7.10 to 7.56 g. We note that the increase in mass is likely to result in an increase of torsional stability for conventional CTSH characterized with end circles as described in [22], but the effect of complex cut-out shape on the torsional stiffness of CTSH remains unclear and needs further investigation. In addition, the failure indices are all less than 0.93 when compared to the original design with failure indices larger than 1, indicating that workable safe structures are obtained through optimization. Figure 9c shows the distribution of midsurface strain, midsurface stress, and failure indices with respect to fully folded configurations for the optimal design. Again, we observe that the maximum of all three indices occurs in the cut-out edge regions, implying the importance of cut-out shape optimization for CTSH.

Finally, in Table 4 we show the effect of choice of the safety factor for failure indices on the optimization results. A variety of failure safety factors ranging from 0.90 to 1.0 were used to perform the shape optimization process. Each of the ANN-predicted optimal solutions was validated by performing a high-fidelity FE simulation. As expected, we found that a larger value of safety factor would lead to an overestimate of the optimal performance; e.g., for the cases with $S_f = 0.95$ and 1.0 the true FE calculation for the optimal design has an FI_3 value above 1.0, which indicates that the optimal design is not safe. On the other hand, a smaller value of safety factor results in a conservative optimal solution. For the case with $S_f = 0.90$, it is

Table 2 Comparison of optimization results based on different surrogate models

Parameter	x_1, mm	x_2, mm	x_3, mm	y_1, mm	y_2, mm	Mass, g	$M_d^{\max}$, N · mm	$E_s^{\max}$, mJ	FI_1	FI_2	FI_3
RBF predicting	55.06	71.52	62.98	7.13	5.40	7.518	6199.1	999.9	0.664	0.662	0.930
FE testing	55.06	71.52	62.98	7.13	5.40	7.518	6187.6	998.2	0.754	0.710	0.935
Predict error	— —	— —	— —	— —	— —	0%	0.19%	0.17%	11.94%	6.76%	0.53%
Kriging predicting	54.62	70.31	64.18	6.56	5.00	7.541	6482.5	1048.7	0.635	0.599	0.930
FE testing	54.62	70.31	64.18	6.56	5.00	7.547	6346.6	1061.1	0.824	0.819	1.07
Predict error	— —	— —	— —	— —	— —	0%	2.14%	1.17%	22.94%	26.86%	13.08%
GPR predicting	56.35	72.12	63.24	6.99	5.00	7.522	6210.3	1010.1	0.643	0.601	0.930
FE testing	56.35	72.12	63.24	6.99	5.00	7.524	6267.1	1019.7	0.615	0.762	0.918
Predict error	— —	— —	— —	— —	— —	0%	0.91%	0.94%	4.55%	21.13%	1.31%
ANN predicting	54.90	70.88	61.94	6.66	5.00	7.551	6255.8	1021.7	0.713	0.702	0.930
FE testing	54.90	70.88	61.94	6.66	5.00	7.556	6328.6	1051.2	0.679	0.822	0.920
Predict error	— —	— —	— —	— —	— —	0%	1.15%	2.81%	5.01%	14.60%	1.09%

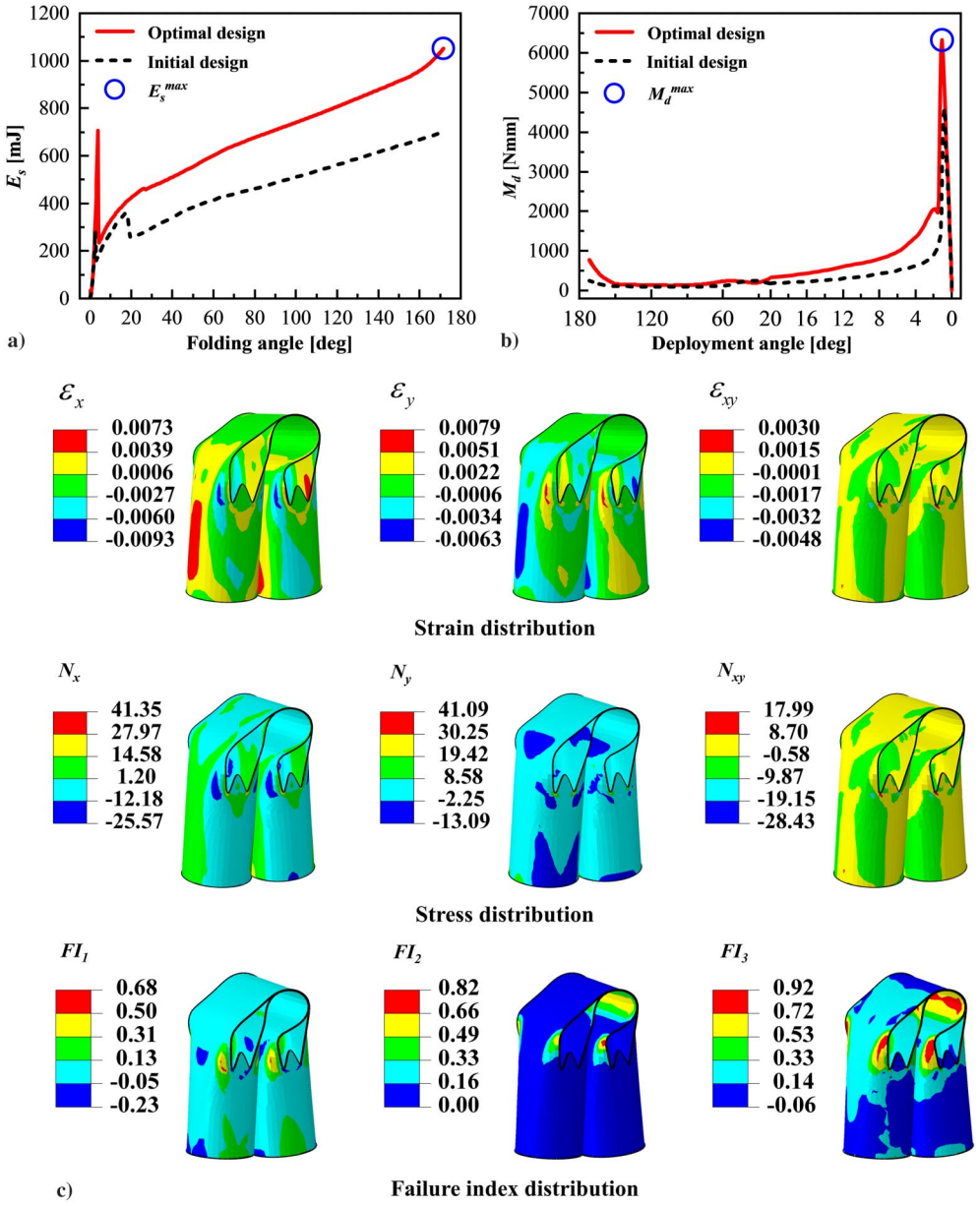

Fig. 9 Comparison of initial and optimal designs: a) $E_s^{\max}$ versus folding angle, b) $M_d^{\max}$ versus deployment angle, and c) distribution of strain, stress, and failure indices.

Table 3 Comparison of initial and optimal design (by ANN) performances

Design	Mass, g	$M_d^{\max}$, N · mm	$E_s^{\max}$, mJ	FI_1	FI_2	FI_3
Initial design	7.10	4638.89	699.98	0.29	1.09	1.08
Optimal design	7.56	6328.60	1051.20	0.68	0.82	0.92
Increment	6.48%	36.42%	50.18%	134.48%	−24.677%	−14.81%

shown that although the value of FI_3 is far less than 1.0, the improvement on the two objective values, $M_d^{\max}$ and $E_s^{\max}$, is also less than the case using $S_f = 0.93$.

VI. Conclusions

Thin-walled composite materials are gaining increasing interest on design and real application of diverse aerospace structures owing to their many unique features. Slots or cut-outs are introduced on purpose into tube, boom, or shell-like thin-walled structures to make these structures be compressed, folded, and stowed for a long period of time, and then release on demand, giving rise to diverse forms of deployable structures. The CTSH considered in this paper is one of the typical examples of deployable composite structures. The boundary shape of the cut-outs is crucial for the CTSH, either from the point view of manufacturing or real application performance. Intensive studies have been taken place on the design, analysis, fabrication, and experiment of folding and deployment of CTSH, but sparse efforts have been devoted to structural optimization of CTSH, although of few works on sizing or topology optimizations. Compared with sizing optimization, shape and topology optimization is of greater importance, but more challenging, and it is yet a topic seldom touched upon.

To perform structural optimization of CTSH, calculating structural response of CTSH is inevitable. For structural optimization problems, hundreds or thousands of iterations are needed; this is

Table 4 Comparison of optimization results based on different safety factors for failure indices

S_f	ANN vs FE	x_1, mm	x_2, mm	x_3, mm	y_1, mm	y_2, mm	Mass, g	$M_d^{\max}$, N · mm	$E_s^{\max}$, mJ	FI_1	FI_2	FI_3
0.90	ANN predicting	54.43	71.19	62.29	6.89	5.00	7.531	6208.6	1001.5	0.665	0.687	0.899
	FE testing	54.43	71.19	62.29	6.89	5.00	7.538	6272.1	1028.8	0.620	0.704	0.879
	Predict error	— —	— —	— —	— —	— —	0%	0.99%	2.65%	7.26%	2.41%	2.28%
0.93	ANN predicting	54.90	70.88	61.94	6.66	5.00	7.551	6255.8	1021.7	0.713	0.702	0.930
	FE testing	54.90	70.88	61.94	6.66	5.00	7.556	6328.6	1051.2	0.679	0.822	0.920
	Predict error	— —	— —	— —	— —	— —	0%	1.15%	2.81%	5.01%	14.60%	1.09%
0.95	ANN predicting	57.37	66.39	61.98	7.43	5.06	7.588	6471.2	1125.5	0.706	0.555	0.950
	FE testing	57.37	66.39	61.98	7.43	5.06	7.581	6409.2	1108.7	0.808	1.025	1.148
	Predict error	— —	— —	— —	— —	— —	0%	0.97%	1.51%	12.62%	45.85%	17.25%
1.00	ANN predicting	57.16	66.24	62.03	6.88	5.00	7.600	6575.3	1157.5	0.785	0.539	0.999
	FE testing	57.16	66.24	62.03	6.88	5.00	7.605	6548.4	1152.3	0.877	1.001	1.210
	Predict error	— —	— —	— —	— —	— —	0%	0.41%	0.45%	10.49%	46.15%	17.44%

prohibitively time-consuming and computer-intensive if every structural response or objective function evaluation is obtained by running high-fidelity FE analysis. This issue is the biggest concern for folding and deployment analysis of CTSH, which would typically take hours to complete due to the complexity of large deformation, self-contact, and the difficulty of convergence. Constructing a surrogate model via extracting input–output relationship in an approximate yet much cheaper way is vital for the realization of structural optimization of CTSH.

This paper poses and formulates the multi-objective shape optimization problem, and it tackles the problem by integrating data-driven surrogate modeling and shape optimization. We describe the surrogate models, detail the implementation, and discuss the framework and software environment. The framework is comprised of an offline data-driven surrogate modeling process, and an online optimization process, and integrated in a seamless fashion. By performing a fraction of data points on design variables via the optimal Latin hypercube sampling and evaluating structural responses through FE analysis, surrogate models based on RBF, kriging, GPR, and ANN were constructed and compared. The surrogate model was substituted into a GA-based optimizer, and used in lieu of high-fidelity FE analysis to evaluate all objective function during the whole optimization process. For the CTSH shape optimization problem considered here, the method saves 97% of computing time and achieves 50 and 35% gains in terms of maximum stored energy and peak bending moment, respectively.

The developed framework and methodology was applied to and validated by a GA-based gradient-free optimization problems. Another aspect of design sensitivity analysis, which is also time-consuming, is avoided for this gradient-free algorithm. But the surrogate-modeling-aided optimization strategy given here is definitely applicable to both gradient-based and gradient-free optimization problems. The developed framework lays its basis on integration and automation of in-house codes and commercial software, making the framework flexible and versatile to meet various requirements. One possible extension of this work is to apply the framework to investigate the effect of a cut-out shape on the torsional stability of CTSH.

Acknowledgments

This research is supported by the National Natural Science Foundation of China (grants 11972277 and 11772247), and the Fundamental Research Funds for the Central Universities (grant YJ2021137). Ning An also acknowledges the support from the Open Project of State Key Laboratory for Strength and Vibration of Mechanical Structures, Xi'an Jiaotong University (No. SV2021-KF-04). Qilong Jia acknowledges the support from Shanghai Rising-Star Program (19QB1404000).

References

[1] Mobrem, M., and Adams, D. S., "Deployment Analysis of the Lenticular Jointed Antennas Onboard the Mars Express Spacecraft," *Journal of Spacecraft and Rockets*, Vol. 46, No. 2, 2009, pp. 394–402. https://doi.org/10.2514/1.36890

[2] Adams, D. S., and Mobrem, M., "Lenticular Jointed Antenna Deployment Anomaly and Resolution Onboard the Mars Express Spacecraft," *Journal of Spacecraft and Rockets*, Vol. 46, No. 2, 2009, pp. 403–410. https://doi.org/10.2514/1.36891

[3] Yee, J., and Pellegrino, S., "Composite Tube Hinges," *Journal of Aerospace Engineering*, Vol. 18, No. 4, 2005, pp. 224–231. https://doi.org/10.1061/(asce)0893-1321(2005)18:4(224)

[4] Yang, H., Guo, H.-W., Wang, Y., Liu, R.-Q., and Li, M., "Design and Experiment of Triangular Prism Mast with Tape-Spring Hyperelastic Hinges," *Chinese Journal of Mechanical Engineering*, Vol. 31, No. 1, 2018, pp. 1–10. https://doi.org/10.1186/s10033-018-0242-5

[5] Silver, M., Hinkle, J., and Peterson, L., "Modeling of Snap-Back Bending Response of Doubly Slit Cylindrical Shells," *45th AIAA/ASME/ASCE/AHS/ASC Structures, Structural Dynamics & Materials Conference*, AIAA Paper 2004-1820, 2004. https://doi.org/10.2514/6.2004-1820

[6] Silver, M., Hinkle, J., and Peterson, L., "Controlled Displacement Snap-Through of Tape Springs: Modeling and Experiment," *46th AIAA/ASME/ASCE/AHS/ASC Structures, Structural Dynamics and Materials Conference*, AIAA Paper 2005-2314, 2005. https://doi.org/10.2514/6.2005-2314

[7] Footdale, J., Banik, J., and Murphey, T., "Design Developments of a Non-Planar Deployable Structure," *51st AIAA/ASME/ASCE/AHS/ASC Structures, Structural Dynamics, and Materials Conference*, AIAA Paper 2010-2608, 2010. https://doi.org/10.2514/6.2010-2608

[8] Ferraro, S., and Pellegrino, S., "Topology and Shape Optimization of Ultrathin Composite Self-Deployable Shell Structures with Cutouts," *AIAA Journal*, Vol. 59, No. 9, 2021, pp. 3696–3709. https://doi.org/10.2514/1.j059550

[9] Seffen, K., and Pellegrino, S., "Deployment Dynamics of Tape Springs," *Proceedings of the Royal Society of London. Series A: Mathematical, Physical and Engineering Sciences*, Vol. 455, No. 1983, 1999, pp. 1003–1048. https://doi.org/10.1098/rspa.1999.0347

[10] Seffen, K., You, Z., and Pellegrino, S., "Folding and Deployment of Curved Tape Springs," *International Journal of Mechanical Sciences*, Vol. 42, No. 10, 2000, pp. 2055–2073. https://doi.org/10.1016/s0020-7403(99)00056-9

[11] Li, F., Liu, L., Du, L., Liu, Y., and Leng, J., "Mechanical Analysis of a Tip-Loaded Deployable Truss Based on Shape Memory Polymer Composite," *Composite Structures*, Vol. 242, June 2020, Paper 112196. https://doi.org/10.1016/j.compstruct.2020.112196

[12] Lakshmi, S. S., Varsha, M., Krishnaa, G. S., Kuriakose, V. M., Subhani, S. M., Subramanian, H. S., and Sreehari, V., "Thermo-Structural Analysis of Deployable Composite Booms with Slotted Hinges for Space Applications," *Materials Today: Proceedings*, Vol. 56, No. 6, 2022, pp. 3564-3. https://doi.org/10.1016/j.matpr.2021.11.633

[13] Mallikarachchi, H., and Pellegrino, S., "Quasi-Static Folding and Deployment of Ultrathin Composite Tape-Spring Hinges," *Journal of Spacecraft and Rockets*, Vol. 48, No. 1, 2011, pp. 187–198. https://doi.org/10.2514/1.47321

[14] Jia, Q., An, N., Ma, X., and Zhou, J., "Exploring the Design Space for Nonlinear Buckling of Composite Thin-Walled Lenticular Tubes Under

Pure Bending," *International Journal of Mechanical Sciences*, Vol. 207, Oct. 2021, Paper 106661.
https://doi.org/10.1016/j.ijmecsci.2021.106661

[15] Mallikarachchi, H., and Pellegrino, S., "Deployment Dynamics of Ultrathin Composite Booms with Tape-Spring Hinges," *Journal of Spacecraft and Rockets*, Vol. 51, No. 2, 2014, pp. 604–613.
https://doi.org/10.2514/1.a32401

[16] Yee, J., and Pellegrino, S., "Biaxial Bending Failure Locus for Woven-Thin-Ply Carbon Fibre Reinforced Plastic Structures," *46th AIAA/ASME/ASCE/AHS/ASC Structures, Structural Dynamics and Materials Conference*, AIAA Paper 2005-1811, 2005.
https://doi.org/10.2514/6.2005-1811

[17] Mallikarachchi, H., and Pellegrino, S., "Failure Criterion for Two-Ply Plain-Weave CFRP Laminates," *Journal of Composite Materials*, Vol. 47, No. 11, 2013, pp. 1357–1375.
https://doi.org/10.1177/0021998312447208

[18] Zhou, Y., Lu, Z., and Yang, Z., "Progressive Damage Analysis and Strength Prediction of 2D Plain Weave Composites," *Composites Part B: Engineering*, Vol. 47, April 2013, pp. 220–229.
https://doi.org/10.1016/j.compositesb.2012.10.026

[19] Li, B., Ye, H., and Zhang, Y., "Failure Analysis of Composite Tube Hinge and Optimization Design," *IOP Conference Series: Materials Science and Engineering*, Vol. 531, March 2019, Paper 012062.
https://doi.org/10.1088/1757-899x/531/1/012062

[20] "Antenna Deployment Arm with Integrated Elastic Hinges," Statement of work AO8702, ESA, 2016, pp. 1–37, https://artes.esa.int/funding/antenna-deployment-arm-integrated-elastic-hinges-artes-ref-5b163-expro.

[21] Fernandes, P., Pinto, R., and Correia, N., "Design and Optimization of Self-Deployable Damage Tolerant Composite Structures: A Review," *Composites Part B: Engineering*, Vol. 221, Sept. 2021, Paper 109029.
https://doi.org/10.1016/j.compositesb.2021.109029

[22] Mallikarachchi, H., and Pellegrino, S., "Design of Ultrathin Composite Self-Deployable Booms," *Journal of Spacecraft and Rockets*, Vol. 51, No. 6, 2014, pp. 1811–1821.
https://doi.org/10.2514/1.a32815

[23] Ye, H., Zhang, Y., Yang, Q., Xiao, Y., Grandhi, R. V., and Fischer, C. C., "Optimal Design of a Three Tape-Spring Hinge Deployable Space Structure Using an Experimentally Validated Physics-Based Model," *Structural and Multidisciplinary Optimization*, Vol. 56, No. 5, 2017, pp. 973–989.
https://doi.org/10.1007/s00158-017-1810-5

[24] Yang, H., Liu, R., Wang, Y., Deng, Z., and Guo, H., "Experiment and Multiobjective Optimization Design of Tape-Spring Hinges," *Structural and Multidisciplinary Optimization*, Vol. 51, No. 6, 2015, pp. 1373–1384.
https://doi.org/10.1007/s00158-014-1205-9

[25] Liu, T.-W., Bai, J.-B., Fantuzzi, N., Bu, G.-Y., and Li, D., "Multi-Objective Optimisation Designs for Thin-Walled Deployable Composite Hinges Using Surrogate Models and Genetic Algorithms," *Composite Structures*, Vol. 280, Jan. 2022, Paper 114757.
https://doi.org/10.1016/j.compstruct.2021.114757

[26] Keane, A., Forrester, A., and Sobester, A., *Engineering Design via Surrogate Modelling: A Practical Guide*, AIAA, Reston, VA, 2008, pp. 49–59.
https://doi.org/10.2514/4.479557

[27] Simpson, T. W., Mauery, T. M., Korte, J. J., and Mistree, F., "Kriging Models for Global Approximation in Simulation-Based Multidisciplinary Design Optimization," *AIAA Journal*, Vol. 39, No. 12, 2001, pp. 2233–2241.
https://doi.org/10.2514/3.15017

[28] Jeong, S., Murayama, M., and Yamamoto, K., "Efficient Optimization Design Method Using Kriging Model," *Journal of Aircraft*, Vol. 42, No. 2, 2005, pp. 413–420.
https://doi.org/10.2514/6.2004-118

[29] Queipo, N. V., Haftka, R. T., Shyy, W., Goel, T., Vaidyanathan, R., and Tucker, P. K., "Surrogate-Based Analysis and Optimization," *Progress in Aerospace Sciences*, Vol. 41, No. 1, 2005, pp. 1–28.
https://doi.org/10.1016/j.paerosci.2005.02.001

[30] Viana, F. A., Simpson, T. W., Balabanov, V., and Toropov, V., "Special Section on Multidisciplinary Design Optimization: Metamodeling in Multidisciplinary Design Optimization: How Far have We Really Come?" *AIAA Journal*, Vol. 52, No. 4, 2014, pp. 670–690.
https://doi.org/10.2514/1.j052375

[31] Jia, Q., An, N., Ma, X., and Zhou, J., "A Dynamic Finite Element Procedure for Bending Collapse of Composite Thin-Walled Lenticular Tubes," *Composite Structures*, Vol. 287, May 2022, Paper 115364.
https://doi.org/10.1016/j.compstruct.2022.115364

[32] Mallikarachchi, H., "Thin-Walled Composite Deployable Booms with Tape-Spring Hinges," Ph.D. Thesis, Univ. of Cambridge, Cambridge, England, U.K., 2011.
https://doi.org/10.2514/6.2011-2019

[33] Wang, G., Sun, S., Li, M., and Zhou, J., "Large Deformation Shape Optimization of Cut-Mediated Soft Mechanical Metamaterials," *Materials Research Express*, Vol. 6, No. 5, 2019, Paper 055802.
https://doi.org/10.1088/2053-1591/aaeabc

[34] Zou, W., Zhou, J., Zhang, Z., and Li, Q., "A Truly Meshless Method Based on Partition of Unity Quadrature for Shape Optimization of Continua," *Computational Mechanics*, Vol. 39, No. 4, 2007, pp. 357–365.
https://doi.org/10.1007/s00466-006-0032-2

[35] *Statistics and Machine Learning Toolbox*, MATLAB, MathWorks, Inc., Natick, MA, 2019.

[36] Williams, C. K., and Rasmussen, C. E., *Gaussian Processes for Machine Learning*, Vol. 2, MIT Press, Cambridge, MA, 2006, pp. 79–102.
https://doi.org/10.7551/mitpress/3206.001.0001

[37] Tripathy, R. K., and Bilionis, I., "Deep UQ: Learning Deep Neural Network Surrogate Models for High Dimensional Uncertainty Quantification," *Journal of Computational Physics*, Vol. 375, Dec. 2018, pp. 565–588.
https://doi.org/10.1016/j.jcp.2018.08.036

[38] Goodfellow, I., Bengio, Y., and Courville, A., *Deep Learning*, MIT Press, Cambridge, MA, 2016, pp. 168–224.
https://doi.org/10.7551/mitpress/11171.001.0001

[39] Keane, A. J., and Voutchkov, I. I., "Surrogate Approaches for Aerodynamic Section Performance Modeling," *AIAA Journal*, Vol. 58, No. 1, 2020, pp. 16–24.
https://doi.org/10.2514/1.j058687

P. Weaver
Associate Editor